

Eigenvalues and Eigenvectors of the Staggered Dirac Operator at Finite Temperature

R. V. Gavai* and Sourendu Gupta†
*Department of Theoretical Physics,
 Tata Institute of Fundamental Research,
 Homi Bhabha Road, Mumbai 400005, India.*

R. Lacaze‡
*Service de Physique Theorique, CEA Saclay,
 F-91191 Gif-sur-Yvette Cedex, France.*

We examine the eigenvalues and eigenvectors of the staggered Dirac operator on thermal ensembles created in QCD with two flavours of staggered quarks. We see that across the phase transition a gap opens in the spectrum. For finite volume lattices in the low-temperature phase the eigenvectors are extended, but generic field configurations in the high temperature phase give rise to localized eigenstates. We examine measures of the stability of such localization and find that at finite volumes localization occurs through Mott's mechanism of the formation of mobility edges. However, the band gap between the localized and extended states seem to scale to zero in the limit of large volume.

PACS numbers: 11.15.Ha, 12.38.Mh

I. INTRODUCTION

Any fermionic operator can be written in the spectral form

$$\hat{\mathcal{O}} = \sum_{\lambda\mu} O_{\mu\lambda} |\lambda\rangle\langle\mu|, \quad (1)$$

where $|\lambda\rangle$ is an eigenvector of the Dirac operator with eigenvalue λ , evaluated separately on each configuration. Typical operators of interest contain quark loops with various insertions, i. e., $\mathcal{O} = \text{Tr} (A_1(D+m)^{-1} A_2(D+m)^{-1} \cdots A_n(D+m)^{-1})$. As a result,

$$\mathcal{O} = \sum_{\lambda_1 \cdots \lambda_n} \frac{\langle\lambda_1|A_1|\lambda_2\rangle\langle\lambda_2|A_2|\lambda_3\rangle\cdots\langle\lambda_n|A_n|\lambda_1\rangle}{\prod_{i=1}^n (m + \lambda_i)}, \quad (2)$$

where we use the symbol D to refer to the massless Dirac operator. If the A_i commute with D , then the matrix elements in the numerator are diagonal, and all questions about the operator reduce to the simultaneous eigenvalues of the A_i and the Dirac operator. This happens, for example, in the chiral sector of the theory, where one deals with questions about n-point functions of pions. Since $\gamma_5 D \gamma_5 = D^\dagger$, most questions about the chiral sector can be answered if the eigenvalues are known. As a result, the thrust of many previous studies of QCD to date has been on the spectrum of eigenvalues, particularly on comparisons with random matrix theory (RMT) [1]. This focus is due to the fact that RMT is known to be equivalent to chiral perturbation theory in some limits [2].

However, at finite temperature, especially above T_c , chiral perturbation theory is not the appropriate long-distance effective theory. Furthermore, there are interesting questions at many different length scales and one may need to build different effective theories to answer these questions. Several questions involve fermionic loops with insertions of operators which do not commute with D . An example is the vector susceptibility,

$$\chi_V = \sum_{\lambda_1, \lambda_2} \frac{|\langle\lambda_1|\gamma_\mu|\lambda_2\rangle|^2}{(m + \lambda_1)(m + \lambda_2)}, \quad (3)$$

which includes quark number susceptibilities. Deeper understanding of such quantities need the study of the eigenvectors [3].

*Electronic address: gavai@tifr.res.in

†Electronic address: sgupta@tifr.res.in

‡Electronic address: Robert.Lacaze@cea.fr

II. EIGENVALUES

We analyzed configurations generated in the study of QCD with two flavours of dynamical staggered quarks at a lattice spacing $a = 1/4T$ [4]. The scale fixing yielded $T_c/m_\rho = 0.186 \pm 0.006$. As T varied between $0.75T_c$ and $2T_c$, the renormalized quark mass was kept constant. The physical box size, $L = N_s a$ where N_s is the box size in units of the lattice spacing. The aspect ratio was varied in the range $2 \leq LT \leq 6$.

We investigated the eigenvalues, λ , and eigenvectors, $|\lambda\rangle$, of the massless Dirac operator, D , in typical thermal ensembles picked from these simulations. We used five configurations separated by two autocorrelation times at all temperatures and volumes except at $1.05T_c$ where we verified the results using twenty configurations. Eigenvalues and eigenvectors were computed with the ARPACK subroutines [5]. For convergence, the tolerance is chosen so that

$$|r|^2 < \epsilon, \quad \text{where} \quad r = (D - \lambda)\psi_\lambda, \quad (4)$$

where λ is an eigenvalue and ψ_λ is the corresponding eigenvector. We report results with $\epsilon = 2 \times 10^{-13}$.

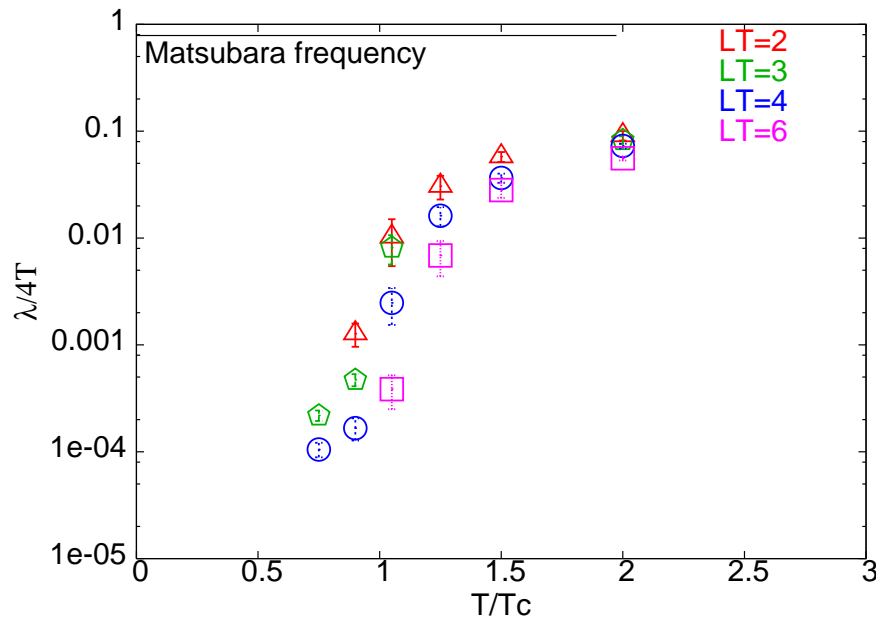


FIG. 1: The lowest Dirac eigenvalues as a function of T for different spatial lattices. In all cases the lattice spacing $a = 1/4T$. Also shown is the lowest Matsubara frequency expected at this cutoff, *i. e.*, the expectation for free fermions.

The lowest staggered Dirac eigenvalue, λ_0 , evolves as shown in Figure 1. There is a clear crossover from low to high temperature behaviour evidenced by an increase in the lowest eigenvalue by three order of magnitude in the neighbourhood of T_c . This becomes sharper in the neighbourhood of T_c with increasing spatial size of the lattice.

It is also worth noting that at $2T_c$ there seems to be little remaining volume dependence. It is interesting that this large volume behaviour sets in at a minimum L given by $L\lambda_0 \approx 0.8$. Consistent with this observation, at $1.5T_c$ the lattice sizes which satisfy this condition also give results which are almost volume independent.

In Figure 1 we further show the lowest eigenvalue of the free Dirac operator on a lattice of the same coarseness. In the limit of zero lattice spacing this would correspond to the Matsubara frequency, $\Omega = \pi T$. The full QCD configurations can be seen to lie very far from the free field theory (ideal gas) limit at all temperatures up to $2T_c$. This is consistent with another observation at the same lattice spacing that the pseudoscalar screening correlator constructed with staggered Dirac quarks yields a screening mass far below that expected from the free theory [6]. It would be interesting to see whether this correlation, related to the chiral behaviour, changes in the same way due to various improvements in the gauge and fermion actions and in the continuum limit.

The Banks-Casher formula [7] relates the density of Dirac eigenvalues at zero with the chiral condensate. In order to utilize this formula we expand the cumulative distribution of the eigenvalues in the form

$$I(x) = \int_0^x d\lambda \rho(\lambda) = \sum_{n \geq 1} a_n x^n, \quad \text{from which} \quad \rho(x) = \sum_{n \geq 1} n a_n x^{n-1}. \quad (5)$$

| Lattice | cutoff | N points | χ^2/N | a_1 | a_2 | a_3 |
|-----------------|-------------------------------|---------------------------|------------|-----------|-----------|----------------------|
| 4×16^3 | 0.01 0.06 | 189 1147 | 0.77 | 0.153(3) | 0.050(50) | 0.8(1.0) 1.9(1.0) |
| | | | 0.37 | 0.153(2) | | |
| | | | 0.20 | 0.152(2) | | |
| | | | 0.17 | 0.152(2) | | |
| | | | 0.15 | 0.153(2) | | |
| 4×12^3 | 0.02 0.06 0.14 | 153 469 1176 | 1.00 | 0.147(2) | 0.116(26) | 0.79(23) 0.49(23) |
| | | | 0.69 | 0.148(2) | | |
| | | | 5.17 | 0.153(2) | | |
| | | | 0.27 | 0.144(2) | | |
| | | | 0.20 | 0.147(2) | | |
| 4×8^3 | 0.06 0.08 0.10 0.375 | 128 172 222 1150 | 0.17 | 0.135(11) | 0.196(26) | 0.43(8) 0.05(8) |
| | | | 0.16 | 0.136(10) | | |
| | | | 0.23 | 0.138(10) | | |
| | | | 6.80 | 0.175(7) | | |
| | | | 0.04 | 0.126(7) | | |
| | | | 0.28 | 0.144(7) | 0.175(25) | |
| | | | 0.03 | 0.128(7) | | |

TABLE I: Fits of the cumulative density for $\beta = 5.26$, i. e., $T/T_c = 0.90 \pm 0.01$.

where the γ_5 -Hermiticity of the staggered Dirac operator as well as its anti-Hermitean nature have been used. Together they imply that the eigenvalues are paired and imaginary, $\pm i\lambda$. The integration above is over the positive λ values. Note that the reflection symmetry in λ permits the existence of an a_2 term (even n , in general) only if the $\rho(\lambda)$ is non-analytic at the origin.

The cumulative distribution was constructed numerically and fitted to the form in eq. (5) for configurations above and below T_c . Indicative results are shown in Tables I and II. The tables are arranged in increasing order of N , the number of eigenvalues included, and n of eq.(5). Note that below T_c one gets a good determination of a_1 for cutoffs of the order of 0.1 or so. In fact, the values of a_1 do not depend on n or N . With increasing lattice size, L , the estimate of a_1 increases marginally. On the larger lattices a_2 is compatible with zero, indicating that the distribution is analytic.

Above T_c , a_2 is clearly non-zero for all cut-offs while a_1 drops with increasing L . This behaviour, shown in Table II, implies that a non-analyticity develops in the spectral density. This non-analyticity is due to the formation of a gap— the spectral density is exactly zero upto the gap, and then becomes non-zero. Another way to test this would be to introduce a gap explicitly in the eq. (5),

$$\rho(x) = \sum_{n \geq 1} n a_n (x - x_0)^{n-1}. \quad (6)$$

Indeed, when one does that, a non-zero value of the gap, x_0 , is observed for those temperatures where a_2 is non-zero by the other method.

III. EIGENVECTORS AND MEASURES OF LOCALIZATION

The eigenvectors of the Dirac equation, ψ , are often investigated through the localized moments

$$P_n^\gamma(\lambda) = V^{n-1} \sum_r |p_\gamma(r; \lambda)|^n, \quad \text{where} \quad p_\gamma(r; \lambda) = \langle \lambda | \gamma | \lambda \rangle, \quad \text{and} \quad P_1^1 = 1, \quad (7)$$

γ is a matrix in Dirac space [10], the inner product in the definition of $p_\gamma(r; \lambda)$ involves a sum over spin-flavour and colour indices, the explicit sum is over all V lattice sites r , and the normalization of the eigenvectors, P_1^1 involves the density where the Dirac matrix is identity. For staggered quarks one has the identity $P_n^1 = P_n^{\gamma_5}$. The second moment,

| Lattice | cutoff | N points | χ^2/N | a_1 | a_2 | a_3 |
|-----------------|-----------------|----------|------------|------------|-----------|-----------|
| 4×24^3 | 0.0025 | 33 | 0.20 | 0.030(3) | | |
| | 0.01 | 140 | 0.22 | 0.032(3) | | |
| | 0.031 | 535 | 0.04 | 0.030(3) | 0.41(5) | |
| | 0.031 | 535 | 0.03 | 0.031(3) | 0.25(10) | 5(2) |
| | 4×16^3 | 22 | 0.38 | 0.0148(36) | | |
| | | 323 | 5.35 | 0.0317(36) | | |
| | | | 1.89 | | 0.81(9) | |
| | | | 0.03 | 0.0125(37) | 0.53(9) | |
| | 0.12 | 1077 | 0.03 | 0.0136(33) | 0.503(37) | |
| | | | 1.27 | 0.029(3) | | 3.4(0.4) |
| | | | 0.01 | 0.0118(32) | 0.57(4) | -0.5(4) |
| 4×12^3 | 0.02 | 20 | 0.57 | 0.0135(45) | | |
| | 0.06 | 130 | 4.06 | 0.0291 | | |
| | | | 0.05 | 0.0060(46) | 0.62(11) | |
| | 0.20 | 1068 | 31.2 | 0.0767 | | |
| | | | 0.13 | 0.0147(39) | 0.45(3) | |
| | | | 2.18 | 0.039(4) | | 1.77(16) |
| | | | 0.01 | 0.008(4) | 0.581(26) | -0.55(16) |
| 4×8^3 | 0.01 | 9 | 0.09 | 0.047(25) | | |
| | 0.02 | 19 | 0.11 | 0.053(24) | | |
| | 0.06 | 68 | 0.16 | 0.064(18) | | |
| | | | 0.03 | 0.048(18) | 0.414 | |
| | 0.20 | 373 | 0.01 | 0.052(11) | 0.348(26) | |
| | 0.415 | 1160 | 0.05 | 0.062(7) | 0.29(2) | |
| | | | 0.003 | 0.051(7) | 0.38(2) | -0.16(6) |

TABLE II: Fits of the cumulative density for $\beta = 5.30$, *i. e.*, $T/T_c = 1.05 \pm 0.01$.

$n = 2$ is called the inverse participation ratio (IPR). The moments P_n^1 have the interesting property that for constant $\psi = 1/\sqrt{V}$, one finds $P_n^1 = 1$, whereas for the localized $\psi(r) = \delta_{r,r_0}$, one has $P_n^1 = V^{n-1}$.

Histograms of IPR against λ are shown in Figure 2. There is a very clear difference between the IPR observed below and above T_c . Below T_c the IPRs are close to unity, without any clear dependence on the eigenvalues. In contrast, the situation is dramatically different above T_c ; several eigenvectors have very large values of IPR. There is correlation between the eigenvalue and IPR, with larger eigenvalues coming with substantially smaller IPR.

Below T_c there is little sign of volume dependence of the IPR, consistent with the small values seen there. Above T_c the smaller IPR values seen for large λ are also volume independent. However, as shown in Figure 2, larger values of IPR are volume dependent. A test of scaling shows that the lattice size dependence is consistent with a power behaviour, L^α , with $2.5 \leq \alpha \leq 3.5$. Again, this is not unexpected, since IPR is constructed to be proportional to the volume for localized eigenvectors.

In [3] the transition from volume dependent to independent values of IPR is used to locate the “mobility edge”. By this identification one would have a mobility edge at $\lambda \simeq 1.25T_c$ for a temperature of $2T_c$. However, the notion of a mobility edge contains more physics and we shall examine it more critically in a later section.

The eigenvalues and eigenvectors of the Dirac operator are clearly dependent on the gauge field backgrounds. However, thermodynamic quantities constructed from these have fluctuations which decrease rapidly with increasing lattice size. The IPR is not such a variable: its fluctuations are comparable to the average, as can be seen in Figure 3. The ratio of the variance and mean of P_2^1 , as a function of λ at $2T_c$, is of order unity [11]. The localization properties of Dirac eigenfunctions can therefore serve to classify the ensemble of gauge configurations which give important contributions to the thermal path integral. This is an obvious statement for overlap quarks, where localized chiral eigenvectors of the overlap Dirac operator are closely connected to localized gauge field configurations which are taken to be the lattice analogue of instantons. It is interesting that localization using staggered quarks, where the connection to topology is obscure, can also be used as a tool for analysis of gauge configurations.

The notion of localization has been closely examined in [8]. Since $p_1(r)$ is non-negative and normalized to unity

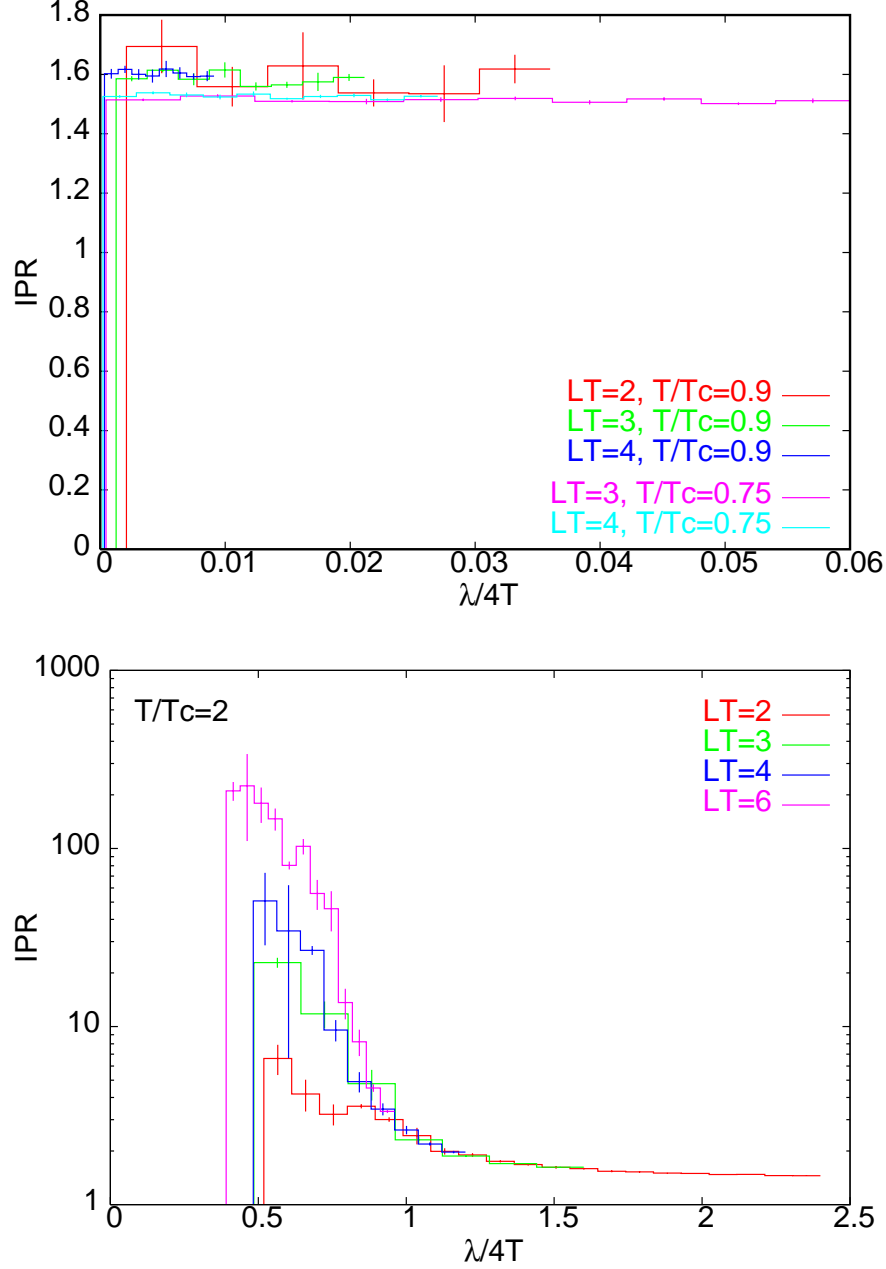


FIG. 2: The IPR, P_2^1 , above and below T_c as a function of the staggered Dirac eigenvalue λ .

one can construct a measure of localization in the following way. Take a value p_f and find the fraction of the lattice sites, $f(p_f)$, containing values $p_1(r) > p_f$. Clearly $f(p_f)$ lies between 0 and 1, and is a decreasing function of p_f . The integral of $p_1(r)$ over these sites, $\mathcal{C}(p_f)$, lies between 0 and 1, and is another decreasing function of p_f . Eliminating p_f between these two, one obtains Horvath's localization function $f(\mathcal{C})$. Clearly $f(\mathcal{C} = 0) = 0$, $f(\mathcal{C} = 1) = 1$ and the function is non-decreasing.

If $p_1(r)$ is highly peaked, then $\mathcal{C}(p_f)$ increases rapidly as p_f decreases, whereas $f(p_f)$ increases slowly. As a result, $f(\mathcal{C})$ is small over most of the range of \mathcal{C} as increases very rapidly to unity near the end of the range. If, on the other hand, $p_1(r)$ is fairly uniform, then both $\mathcal{C}(p_f)$ and $f(p_f)$ increase fairly abruptly over a small range of p_f . The function $f(\mathcal{C})$ then increases very rapidly towards unity at small \mathcal{C} . In Figure 4 we show the behaviour of several models of $p_1(r)$ —

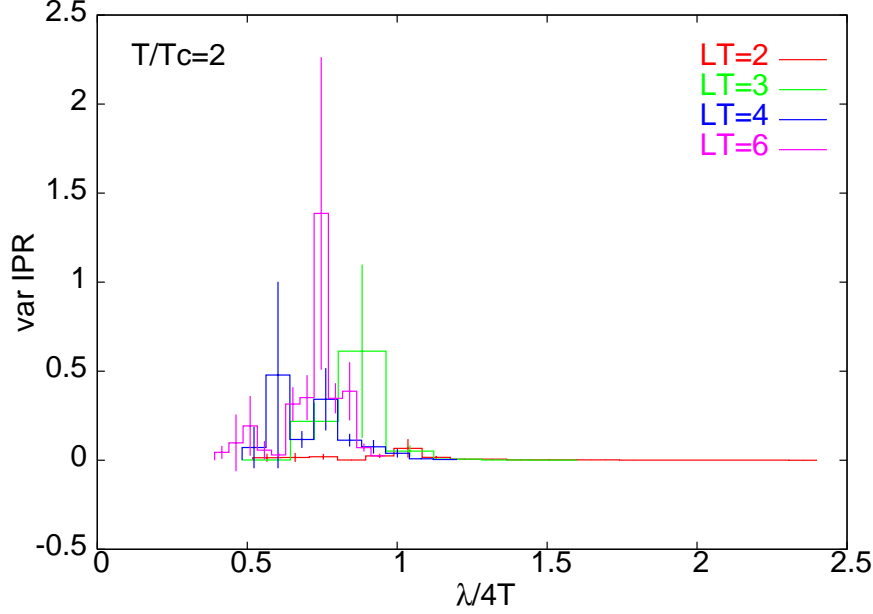


FIG. 3: The relative fluctuations in the IPR, *i. e.*, the ratio of the variance and the mean, at $2T_c$ as a function of the staggered Dirac eigenvalue, λ .

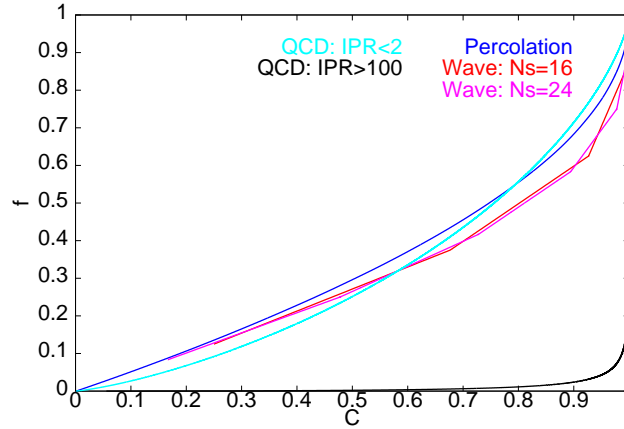


FIG. 4: Examples of the localization function, $f(C)$, for different models of localization, compared with two examples from QCD.

1. Some periodic functions, $\cos^2(k \cdot r)$, normalized to unity on two lattices; these have $P_2^1 = 1.5$.
2. Random uncorrelated function values on sites, drawn from the uniform distribution in $[0, 1]$, normalized to unity; these have $P_2^1 = 1.66$.
3. Two Dirac eigenvectors obtained from the same gauge configuration at $2T_c$, one with $P_2^1 < 2$ and the other with $P_2^1 > 100$.

The localization function $f(C)$ clearly contains more information than the single number P_2^1 , *i. e.*, the IPR. However, the IPR is statistically compatible with statements obtained from the more detailed measurement of $f(C)$. We demonstrate this by the following correspondence. Choose any arbitrary value, C_* , the function value $f(C_*)$ is strongly correlated with the IPR, as we show in Figure 5. For a wide range of C_* we find $f(C_*) \propto 1/P_2^1$.

We give an example of a question which can be easily answered through the use of the localization function. If the eigenvector is localized, then how does it fall off away from the peak? Exponential fall, $\psi(r) \simeq \exp(-\alpha R)$, where R

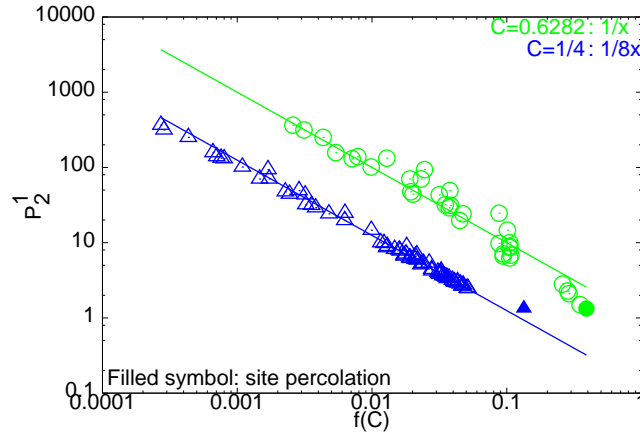


FIG. 5: The strong correlation between IPR, P_2^1 , and the value of the localization function for two values of C shows that the latter contains all the information available in the former.

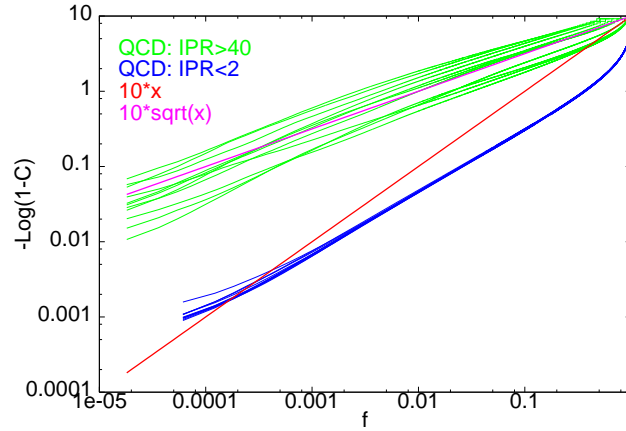


FIG. 6: Scaling of the localization function in the vicinity of $f = C = 1$ shows that staggered Dirac eigenvectors with IPR larger than 40 fall exponentially far from the peak, whereas those with IPR less than 2 have drastically different behaviour.

is the distance from the peak, would imply $C \simeq 1 - g(R) \exp(-R^2)$ and $f \simeq R^d$, in d dimensions. Thus, exponential falloff of a localized eigenvector would give rise to the relation $-\log(1 - C) \propto \sqrt{f}$, for both C and f close to unity. In Figure 6, we show that this is true of staggered Dirac eigenvectors with $P_2^1 > 40$ but those with $P_2^1 < 2$ have completely different behaviour.

A model for eigenvectors with small IPR is that of a function $p_1(r)$ with random uncorrelated values. We call this the site percolation model for the following reason. As we trace out the level curves of this function by choosing p_f , we pick sites independently with a probability given exactly by f . Each site belongs to a unique cluster, defined as the collection of all neighbouring sites on the lattice which are picked [12]. When f is small, we find small localized clusters, but above some critical value, we have percolating clusters. Each realization of the random function is a realization of the percolation problem for all possible probabilities.

As we fill a larger and larger fraction of the lattice, the number of clusters, N_c , grows until the percolation threshold is reached, after which the number of clusters begins to decrease. The clusters are ramified, and, near the critical percolation probability, have a fractal dimension related to the critical indices of the percolation problem. Above the critical probability, the clusters have canonical dimension, as a result of which the holes are filled in rapidly, and N_c decreases.

In Figure 7 we compare the average cluster size as a function of f for the site percolation problem and those eigenvectors in QCD at $2T_c$ which have IPR greater than 2. The fact that QCD has more clusters at larger f than site percolation implies that the percolating cluster constructed from P_2^1 have larger holes inside them where isolated clusters can exist.

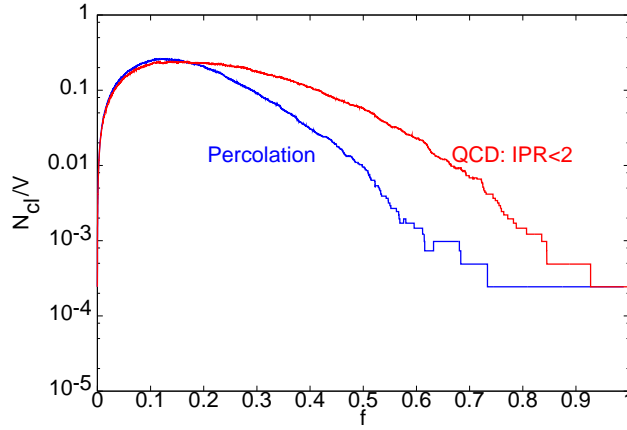


FIG. 7: The number of clusters, N_c , normalized by the lattice volume for uncorrelated site percolation and for those eigenvectors of the staggered Dirac operator at $2T_c$ which have IPR smaller than 2.

IV. STABILITY OF LOCALIZATION

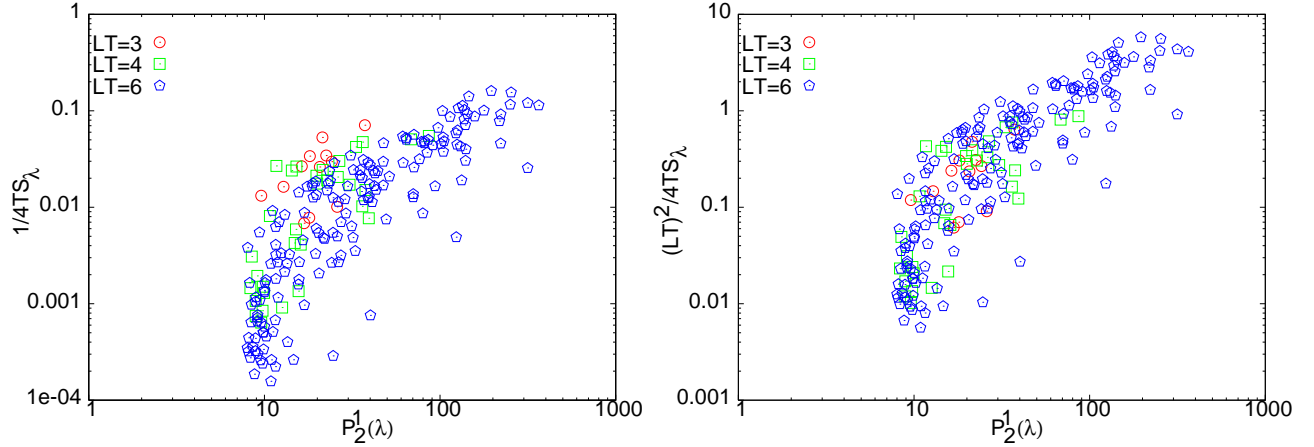


FIG. 8: The stability of localization of staggered Dirac eigenvectors with 2 flavours of dynamical quarks in QCD at $2T_c$. The first panel shows that stability decreases with increasing spatial size. The second shows that the data supports scaling as $1/L^2$.

One of the paradigms in the analysis of Dirac eigenvectors is that of Mott localization and the existence of a mobility edge. In a metallic crystal with random impurities, localization of electron wavefunctions can be observed. Mott argued that if there exist a localized and an extended state arbitrarily close in energy, then they will mix under any small perturbation of the Hamiltonian (induced, for example, by the movement of one of the impurities) hence destroying localization. He argued that, as a result, localization is robust only when localized and extended states are separated in energy. It is well-known that this argument could fail if the extended states have support in regions with holes, since the lack of overlap can then be arranged in space rather than in energy.

The mobility edges are the band edges of localized states. On a finite lattice where the eigenvalue spectrum is discrete, the identification of a mobility edge is not straightforward. As a result, it is hard to test Mott's picture of localization directly. It is interesting to build another measure of stability. We do this next.

Assume that the Dirac operator is perturbed by a change in the gauge fields, $D(U + \delta U) = D(U) + \delta D$. Then, first order perturbation theory tells us that the change in an eigenvector is

$$\delta|\lambda\rangle = \sum_{\lambda'} \mathbf{C}_{\lambda\lambda'} |\lambda'\rangle, \quad \text{where} \quad \mathbf{C}_{\lambda\lambda'} = \frac{\langle \lambda' | \delta D | \lambda \rangle}{\lambda' - \lambda}. \quad (8)$$

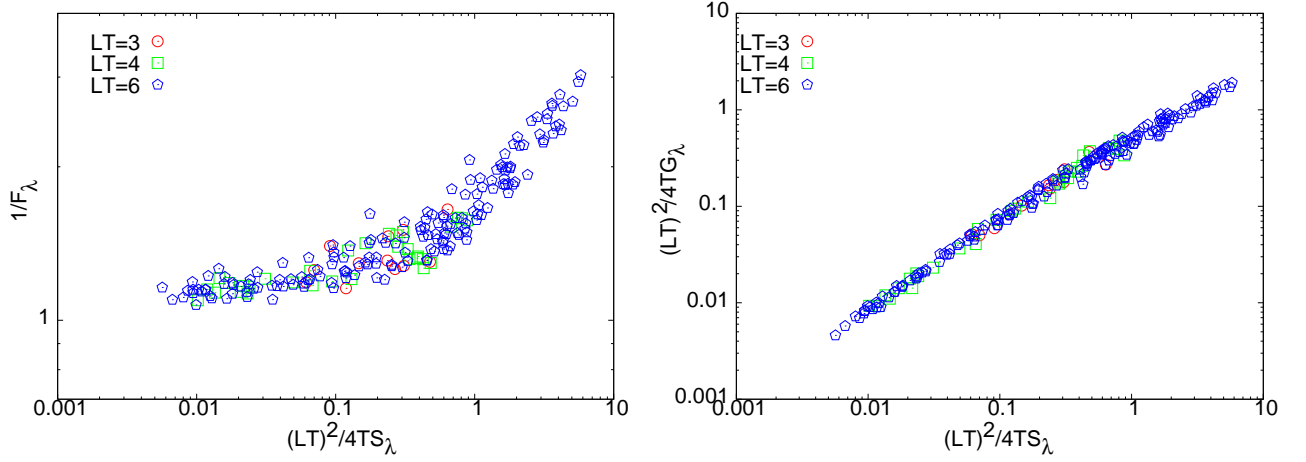


FIG. 9: Correlation between the measures of stability of the localization of staggered Dirac eigenvectors, with 2 flavours of dynamical quarks in QCD at $2T_c$. Note the common scaling of the stability measure \mathcal{S}_λ with the eigenvalue difference \mathcal{G}_λ .

Under a random change of the gauge fields, the phase information in the matrix element above is randomized. Hence, for a study of average properties of the perturbations over ensembles of random changes of gauge field, it would suffice to study $C\delta U$ instead, where

$$C_{\lambda\mu} = \frac{\sum_r \sqrt{p_1(r; \lambda)p_1(r; \mu)}}{|\lambda - \mu|}. \quad (9)$$

This matrix can be extracted purely from the knowledge of the eigenvalues and eigenvectors of the staggered Dirac operator. Note also that the mixing involves both a spatial part, which is the numerator, and a part in energy, which is the denominator. A small mixing can be a result of either.

A perturbing field of $\delta U \simeq 1/C_{\lambda\mu}$ would change $|\lambda\rangle$ by adding to it a significant part of $|\mu\rangle$. As a result, the state $|\lambda\rangle$ is only as stable as the largest value of $C_{\lambda\mu}$. The least stable eigenvector is that for which this measure of stability is minimized. The stability of the localization of Dirac eigenvectors in a given gauge field configuration depends on the least stable localized eigenvector. Hence the stability can be defined to be the quantity

$$\mathcal{S} = \min_{\lambda \in loc} \mathcal{S}_\lambda, \quad \text{where} \quad \mathcal{S}_\lambda = \max_{\mu \in ext} C_{\lambda\mu}, \quad (10)$$

such that the minimum is over states $|\lambda\rangle$ which are localized and the maximum is over states $|\mu\rangle$ which are extended. The inverse, $1/\mathcal{S}_\lambda$, for a localized state $|\lambda\rangle$, is a measure of the minimum field strength which causes significant mixing with an extended state. This measure is eminently suited to a lattice where the spectrum is discrete. If indeed there is stable localization, then examination of the particular element of the mixing matrix which gives \mathcal{S} can help us to identify whether localization is achieved through Mott's mechanism and the formation of mobility edges, or through spatial segregation of the support of localized and extended states.

A numerical implementation of eq. (10) requires specification of which eigenvectors are localized. We use a definition in terms of the IPR, taking all eigenvectors with $P_2^1 > P_2^*$ are localized and those with $P_2^1 < P_2^*$ are deemed to be extended. When changing this definition in the range $2 \leq P_2^* \leq 10$ we found no significant change in the quantities reported below. The data shown in the figures are obtained with $P_2^* = 8$.

In Figure 8, we show stability of the most localized states at $2T_c$ as a function of P_2^1 . The quantity plotted is a dimensionless measure of the minimum change in the gauge field required to mix a given localized state with any extended state— $1/4TS_\lambda$. As shown in the first panel, there is a tendency for $1/4TS_\lambda$ at a given P_2^1 to decrease as the lattice size increases. Scaling the data by a power of the lattice size one finds an optimum scaling as the point where the Fisher's linear discriminant is least able to separate the data for different lattice sizes. In the second panel of the figure we exhibit the resultant scaling with the lattice size, $1/4TS_\lambda \propto (LT)^{-2}$ at fixed P_2^1 . If this scaling persists at larger lattice sizes, then it would imply that in the thermodynamic limit an arbitrarily small change in the gauge field can destabilize the localized eigenvalues.

The scatter in the data does not allow us to measure the scaling exponent more precisely. One could argue that since we are examining localized states, the factor of p_1 in eq. (9) does not scale with volume. In that case one is forced to the conclusion that the observed volume dependence come from the energy differences in the denominator of eq. (9) scale as L^2 . Such a scaling is open to clear tests, and we perform this next.

Since a lattice allows only discrete eigenvalues of the Dirac operator, the origin of localization on the lattice is not a mystery. Nevertheless, one could try to probe the origin in more detail. In order to do this we construct two matrices

$$F_{\lambda\mu} = \sum_r \sqrt{p_1(r;\lambda)p_1(r;\mu)}, \quad \text{and} \quad G_{\lambda\mu} = \frac{1}{|\lambda - \mu|}, \quad (11)$$

one of which, F , looks only at the spatial overlap, and the other, G , only at the overlap in energy. Using these we can define the notions of stability, $\mathcal{F}_\lambda = \max_{\mu \in \text{ext}} F_{\lambda\mu}$ and $\mathcal{G}_\lambda = \max_{\mu \in \text{ext}} G_{\lambda\mu}$.

We found that \mathcal{S}_λ is strongly correlated to both \mathcal{F}_λ and \mathcal{G}_λ . As expected from the earlier argument, \mathcal{F}_λ shows no scaling with L . As a result, it requires no scaling when plotted against the scaled quantity L^2/\mathcal{S}_λ . On the other hand, whereas \mathcal{G}_λ scales with the same exponent as \mathcal{S}_λ . As a result, when plotted against the scaled quantity L^2/\mathcal{S}_λ , one requires the scaling L^2/\mathcal{G}_λ in order for the measurements to be universal. These correlations are shown in Figure 9. From the figures it is clear that the stability of the localization phenomenon seen at finite lattice spacing is controlled by the energy level differences. The situation seems to produce a curious version of Mott's argument. In this case we have localized states whose spatial overlap with extended states is finite. Thus there is no segregation of the spatial support of localized and extended states. Localization is seen at any finite volume, and is realized through the formation of a mobility edge. However the gap between the localized and extended eigenvalues seems to disappear as a power of the lattice volume. As a result there could be no localization in the thermodynamic limit.

One can cross check this conclusion also by computing the minimum of the mobility gap; i. e., the difference between the maximum energy level among the localized states and the minimum energy level between the extended states. This mobility gap scales to zero as $1/(LT)^3$, and the scaling is not sensitive to the choice of P_2^* used to separate localized and extended states in the range $2 \leq P_2^* \leq 10$.

V. CONCLUSIONS

In this paper we have examined the eigenvalues and eigenvectors of the staggered Dirac operator evaluated on thermalized configurations obtained in simulations of QCD with two flavours of dynamical staggered quarks at temperatures between $0.75T_c$ and $2T_c$ with lattice spacing of $a = 1/4T$. The spectrum develops a gap as one crosses T_c , although in the high temperature phase the gap remains substantially smaller than that in free field theory. It would be interesting to study the gap formation in the transition region to check whether this way one can obtain additional insight on the crucial question of the order of the phase transition.

The smallest eigenvalues have eigenvectors which are localized. We investigated different quantities, the inverse participation ratio (IPR) and the localization function, which measure the degree of localization, and found good agreement between them.

We investigated the stability of localization properties of the staggered Dirac eigenvectors with respect to changes in the gauge field background. We showed that localization properties are not stable as one takes the thermodynamic limit. In fact, the scaling of the data shows that in that limit localization of staggered Dirac eigenvectors is not expected to be of thermodynamic importance.

We developed measures of stability which distinguish between stability due to spatial and energy separation of the eigenfunctions. QCD with staggered quarks seems to contain a curious reversal of Mott's argument. The support of localized wavefunctions is not spatially separated from that of extended wavefunctions, and this persists into the thermodynamic limit. As a result, if localization were to be obtained, it would be through the formation of a mobility edge. Indeed, at each volume, one does seem to observe the formation of a mobility edge.

However, localization is spoilt by the fact that the energy denominators can become arbitrarily small, scaling as a power of the spatial volume in the thermodynamic limit where $L \rightarrow \infty$. It would be interesting to extend this work to the overlap Dirac operator, whose exact zero modes are related to localized topological features of gauge field configurations [3].

This work was funded by the Indo-French Centre for the Promotion of Advanced Research under its project number 3104-3. Part of the computations were carried out on the Cray X1 of the Indian Lattice Gauge Theory Initiative (ILGTI).

-
- [1] S. M. Nishigaki *et al.*, *Phys. Rev.*, D 58 (1998) 087704;
J. C. Osborn and J. J. M. Verbaarschot, *Nucl. Phys.*, B 525 (1998) 738;
M. Göckeler *et al.*, *Phys. Rev.*, D 59 (1999) 094503;
F. Farchioni *et al.*, *Nucl. Phys.*, B 549 (1999) 364;

- P. H. Damgaard *et al.*, *Nucl. Phys.*, B 583 (2000) 347, and *Phys. Lett.*, B 495 (2000) 263;
M. Göckeler *et al.*, *Nucl. Phys. Proc. Suppl.*, 94 (2001) 402;
E. Follana *et al.*, *Phys. Rev.*, D 72 (2005) 054501.
- [2] E. V. Shuryak and J. J. M. Verbaarschot, *Nucl. Phys.*, B 560 (1993) 306;
J. J. M. Verbaarschot, *Phys. Rev. Lett.* 72 (1994) 2531.
- [3] L. Venkataraman and G. Kilcup, *Nucl. Phys. Proc. Suppl.*, 63 (1998) 826;
R. G. Edwards and U. M. Heller, *Nucl. Phys. Proc. Suppl.*, 109A (2002) 124;
R. V. Gavai, S. Gupta and R. Lacaze, *Phys. Rev. D* 65 (2002) 094504. C. Bernard *et al.*, *PoS*, LAT2005 (2006) 299;
C. B. Lang *et al.*, hep-lat/0512045.
- [4] R. V. Gavai and S. Gupta, *Phys. Rev.*, D 71 (2005) 114014.
- [5] K. J. Maschhoff and D. C. Sorensen, preliminary proceedings, Copper Mountain Conference on Iterative Methods, 1996,
<http://www.caam.rice.edu/software/ARPACK/>
- [6] K. D. Born *et al.*, *Phys. Rev. Lett.* 67 (1991) 302.
- [7] T. Banks and A. Casher, *Nucl. Phys.* B 169 (1980) 103.
- [8] I. Horvath, *Nucl. Phys.*, B 710 (2005) 464.
- [9] J. Hoshen and R. Kopelman, *Phys. Rev.*, B 14 (1976) 3438.
- [10] Note that P_2^V is needed for the vector susceptibility defined in eq. (3)
- [11] In condensed matter systems, such an observation would lead to a prediction of conductance fluctuations in random media.
- [12] The assignment of sites to clusters is performed by the Hoshen-Kopelman algorithm [9].